Choosing a Model and Appropriate Transition Dipole Moments for Time-Dependent Calculations of Intervalence Electronic Transitions

ARTICLE *in* THE JOURNAL OF PHYSICAL CHEMISTRY · MAY 1996

Impact Factor: 2.78 · DOI: 10.1021/jp951165a

2 AUTHORS, INCLUDING:

Jeffrey I Zink
University of California, Los Angeles
470 PUBLICATIONS **22,143** CITATIONS

SEE PROFILE

Choosing a Model and Appropriate Transition Dipole Moments for Time-Dependent Calculations of Intervalence Electronic Transitions

David S. Talaga and Jeffrey I. Zink*

Department of Chemistry and Biochemistry, University of California, Los Angeles, Los Angeles, California 90095

Received: April 25, 1995; In Final Form: August 3, 1995[⊗]

Intervalence electron transfer spectra in mixed-valence molecules are frequently modeled by an interacting pair of adiabatic potential energy surfaces. The presence or absence of a double minimum in the lower surface is correlated with trapped or delocalized charges, respectively. In the time-dependent picture of the spectroscopy, calculations are conveniently carried out in a diabatic basis. The choice of a diabatic basis for a given adiabatic potential surface is not unique. The appropriateness of a given representation depends on the physical model that is chosen to represent the system. We present three diabatic models that give the same adiabatic potential surface. The first model represents charge transfer between two sites, the second represents a transition between bonding and antibonding molecular orbitals, and the third represents a nonbonding to nonbonding transition. Each of these models gives rise to a different calculated absorption spectrum even though they arise from the same adiabatic picture. A very important consideration after a model is chosen is the selection of the transition dipole moment. We derive and discuss the symmetry of the transition dipole moment for each of the models for the different polarization directions of the incident light and show how the symmetry depends on the choice of the model. Surprisingly, the Condon approximation corresponds to different polarization directions in the different models. We derive the explicit relationships and interconnections between the three models and the adiabatic model.

Introduction

An intervalence absorption spectrum represents an interesting and subtle type of electronic transition where the initial and final states cannot be represented by potential energy surfaces and the Born−Oppenheimer approximation. The intervalence absorption band is a low energy transition in the red or near-IR region of the absorption spectrum that is present in molecules containing two interchangeably equivalent sites with different oxidation states but is absent in molecules where the two sites have the same oxidation state.[1−12] A large number of examples are known where the two sites are metal atoms connected by a bridging ligand; examples of both "linear" and "bent" geometries are known.[13−15] For generality, the only symmetry that we impose on the models is interchange symmetry due to the equivalent sites. In this paper we represent the mixed valence molecule by

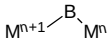

We will also show how to treat the special case of a "linear" molecule.

A simple starting point for representing an intervalence electron transfer spectrum is the pair of adiabatic Born−Oppenheimer potential energy surfaces shown in Figure 1. The intervalence absorption band is treated in terms of a transition from the lower electronic surface (representing the ground state) to the upper electronic surface. The degree of localization of the "extra" charge can be thought of in terms of the barrier in the lower adiabatic surface. A large barrier corresponds to localized behavior. Reducing the barrier results in partially delocalized charge with completely delocalized behavior ensuing when the barrier disappears. The adiabatic potential surfaces have the advantage of presenting a simple physical model for both the electronic transition and the trapping versus delocalization of the charge. However, the latter aspect reveals a serious flaw, especially in the case of trapped charges: the formal charge is very dependent on the nuclear coordinate, and neglecting the coupling of the nuclear and electronic kinetic energy is not satisfactory.

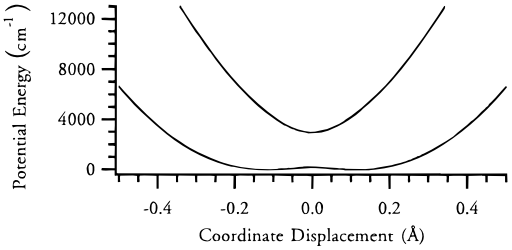

Figure 1. Adiabatic potential energy surfaces for the sample calculations in this paper. Increasing the barrier corresponds to localized behavior while decreasing and eliminating the barrier corresponds to delocalized behavior. The parameters used to generate these potentials as defined in the text are $\Delta Q = 0.15$Å, $k = m\nu^2 2\pi c/\hbar/N_A/10^{23}$, $m = 17$ amu, $\nu = 450$ cm^{-1}, $\epsilon = 1400$cm^{-1}.

The method that we use to surmount this flaw and to calculate the intervalence spectra[16] is based on time-dependent theory of electronic spectroscopy[17−20] and numerical integration of the time-dependent Schrödinger equation.[21−23] The time-dependent theory of absorption spectroscopy between two Born−Oppenheimer surfaces such as the adiabatic surfaces shown in Figure 1 is well developed. The lowest energy vibrational eigenfunction of the lowest energy surface is multiplied by μ, the transition dipole moment, and propagated on the upper surface according to the time-dependent Schrödinger equation. The absorption cross section is the Fourier transform of the autocorrelation function. For an allowed electronic transition, μ is nonzero at the equilibrium nuclear geometry. A common approximation

[⊗] Abstract published in *Advance ACS Abstracts,* April 1, 1996.

S0022-3654(95)01165-8 CCC: $12.00

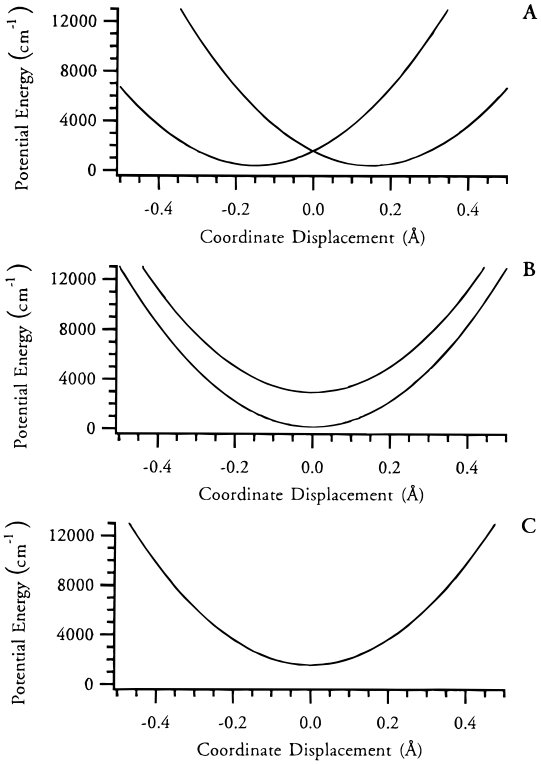

Figure 2. (a) The top panel shows the diabatic basis states for the coordinate-displaced model. The coordinate displaced harmonic potentials are coupled by a constant ($\epsilon = 1400$ cm^{-1}) to give the adiabatics shown in Figure 1. (b) The center panel shows the diabatic basis states for the energy-displaced model. The energy displaced harmonic potentials are coupled by a linear coupling term to give the adiabatic surfaces shown in Figure 1. (c) The bottom panel shows the diabatic basis states for the undisplaced model. The degenerate harmonic potentials are coupled by an even term with a functional form as given in the text to give the adiabatics shown in Figure 1.

is to assume that it is a nonzero constant along the coordinate (the Condon approximation.) For an electric dipole forbidden transition, μ is zero at the equilibrium nuclear geometry, but it may be nonzero at other positions along the coordinate in which case it is "vibronically allowed". When $\mu(q) = -\mu(-q)$, the selection rules are opposite to those in the allowed case.

In the cases of the coupled diabatic potential surfaces shown in Figure 2, the application of time-dependent theory is more detailed. The initial eigenfunction has two components labeled by the two electronic states. The intervalence electron transfer requires that the component labeled by state 1 is multiplied by the transition dipole moment, propagated on state 2, and the component labeled by state 2 is multiplied by the transition dipole moment and propagated on state 1. The absorption cross section is the Fourier transform of the autocorrelation function (Appendix 1). Thus, two components of the wavepacket, including amplitude transfer at each time step, have to be propagated. The functional form of the transition dipole moment that must be used is not intuitively obvious. As we will show, the polarization directions for "allowed" and "forbidden" transitions are different in the different models, and if the Condon approximation is used, the polarization directions are also different. These aspects are not generally appreciated in the literature on the subject.

The focus of this paper is how the investigator's idea of the physical nature of an intervalence transition determines the model that is chosen and therefore influences the calculated spectrum. This paper is divided into three section. In section I we examine three different pairs of diabatic surfaces representing three different models that generate the same adiabatic potential surfaces. Each of these three models is based on a different physical picture of the intervalence transition. The first model represents charge transfer between two sites, the second represents a transition between bonding and antibonding molecular orbitals, and the third represents a nonbonding to nonbonding transition. The specific forms of the couplings required to give the adiabatic potential energy surfaces are derived. In section 2 we treat the transition dipole moments and the spectra for each model. To illustrate physically the functional forms of the transition dipole moments, we use a graphical method pioneered by Tannor for the water molecule. We show that the functional forms, the symmetries and the definitions of allowed and forbidden are dependent on the polarization direction and how they differ for each of the three models. We show how the symmetry of the transition dipole moment depends on the choice of model, and we show how to choose its symmetry to be consistent with the choice of polarization. We show that each of these pictures gives rise to a different absorption spectrum even though specific pairs of the models have the same eigenvalues. Finally, in part 3 we derive the explicit relationships and interconnections between the three models. We illustrate the unitary transformation, eigenvalues, and transition probabilities. Most importantly, we discuss in detail the group theoretical connections between the models. The "vibronic selection rules" are derived, and we show that the presence or absence of a band depends only upon the symmetry and the polarization of the light and does not depend on the model chosen. The spectral intensities are model dependent.

1. Potential Energy Representations for Mixed-Valence Species

We use diabatic Hamiltonians to represent the breakdown of the Born−Oppenheimer approximation. A diabatic Hamiltonian is one in which the nuclear kinetic energy operator is diagonal and the potential energy operator contains the coupling terms.[24−27] Some physical model is used to determine the form of the diabatics; the choice of the diabatic basis is not unique for a finite set of states.[26] In this section we present three different diabatic models which generate the same adiabatic surfaces. Each of the three pairs of diabatic surfaces represents a different physical interpretation of the intervalence transition. Model 1 consists of two identical diabatic surfaces with their minima at the same energy but displaced by equal and opposite distances along the configurational coordinate. Constant coupling generates the standard adiabatic surface. Model 2 consists of two identical diabatic surfaces with their minima at the origin of the configurational coordinate but displaced in energy. Linear coupling that changes sign at the origin generates the standard adiabatic surface. Model 3 consists of two identical diabatic surfaces undisplaced in both energy and coordinate. A specific coordinate dependent coupling that increases symmetrically in both the positive and negative coordinate directions generates the standard adiabatic surface.

Model 1: Coordinate-Displaced Model Representing Localized Charge Transfer. The coordinate-displaced model, shown in Figure 2a, provides a simple and natural way of representing the intervalence charge transfer. One diabatic potential energy surface represents a single valence-localized form of the

$$M^n \overset{B}{\diagup\!\diagdown} M^{n+1}$$

molecule. The other surface represents the other trapped valence form

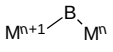

The presence of an extra electron results in the two states having equal and opposite distortions in one or more asymmetric coordinates. A vertical transition from one state to the other corresponds to moving an electron from one site (M^n) to the other (M^{n+1}) without a change in nuclear position. The two electronic configurations are coupled by a constant term ϵ which gives rise to the two adiabatic surfaces. Increasing this coupling parameter results in more delocalized behavior. The potential energy operator is

$$\hat{\mathbf{V}} = \begin{vmatrix} {}^1/_2k(Q + \Delta Q)^2 & \epsilon \\ \epsilon & {}^1/_2k(Q - \Delta Q)^2 \end{vmatrix} \qquad (1)$$

where Q is a non-totally-symmetric coordinate that changes sign under permutation of the identical sites, k is the harmonic force constant and ΔQ is a bond length change along Q in the diabatic representation . If $|\epsilon| < k\Delta Q^2$, the adiabatic surfaces have minima at

$$Q_{\min} = \pm\sqrt{\Delta Q^2 - (\epsilon/k\Delta Q)^2}$$

and a barrier height of

$$V_{\text{barrier}} = (\epsilon - k\Delta Q^2)^2/2k\Delta Q^2$$

If $|\epsilon| \geq k\Delta Q^2$, then there is a single minimum at at $Q = 0$ and no barrier.

The diabatic surfaces represent symmetrically displaced harmonic oscillators.[28] The physical meaning of these surfaces is that there are two equivalent sites for an electron on the molecule and that the molecule can be in either of the two states. Symmetry requires that the coupling term be even in the coordinate Q. A constant is the simplest form meeting this requirement. In the 2×2 matrices, each diagonal element operates on the nuclear part of the wave function from a single diabatic electronic state, whereas the off-diagonal elements transfer population from one state to the other.

Model 2: Energy-Displaced Model Representing Bonding/Nonbonding Transitions. The second set of model diabatics that we will interpret is shown in Figure 2b. The undisplaced diabatic states are separated in energy by 2ϵ. Symmetry requires that these surfaces be coupled by a term which is odd in the coordinate Q. A linear coupling term is the simplest form meeting this requirement. The potential energy operator is

$$\hat{\mathbf{V}} = \begin{vmatrix} {}^1/_2kQ^2 + \epsilon & \Delta QkQ \\ \Delta QkQ & {}^1/_2kQ^2 - \epsilon \end{vmatrix} \qquad (2)$$

The parameters in this model are identical in magnitude and dimension to those of the coordinate-displaced model. A physical meaning for this model has been proposed by Schatz and coworkers.[29] The symmetric and antisymmetric combinations of two orbitals (one from each site) give rise to bonding and antibonding molecular orbitals. The "extra" electron is in the lower energy orbital. By symmetry there cannot be a distortion in this asymmetric coordinate because the orbitals are symmetrized. The presence of the double minimum (or a broadened single minimum) in the adiabatic limit is a result of the linear in coordinate coupling term. Increasing the magnitude of this coupling term results in more localized behavior. A vertical transition from one state to the other corresponds to moving an electron from a bonding to an antibonding orbital without a change in nuclear positions. One problem with this interpretation is that the apparent force constant in the higher energy adiabatic (antibonding orbital) is greater than that in the lower adiabatic (bonding orbital) which is opposite to what one would normally expect.

Model 3: Nondisplaced Model Representing Nonbonding to Nonbonding Transitions. The third diabatic basis consists of two states which are not displaced in either energy or coordinate, e.g., they are degenerate at all nuclear configurations. These two states have some nonzero interaction at the zero of the coordinate which increases with displacement along the coordinate in either direction. Localization of the charge increases as the rate of change of the coupling with respect to the coordinate increases. The potential energy operator for this model is

$$\hat{\mathbf{V}} = \begin{vmatrix} {}^1/_2kQ^2 & \sqrt{(\Delta QkQ)^2 + \epsilon^2} \\ \sqrt{(\Delta QkQ)^2 + \epsilon^2} & {}^1/_2kQ^2 \end{vmatrix} \qquad (3)$$

Figure 2c shows surfaces generated from this equation. The parameters have the same dimensions and magnitudes as those of models 1 and 2. One physical interpretation of this model is that one (or more) orbital(s) on the bridge mediates the interaction of two nonbonding orbitals on the two equivalent sites. As the molecule vibrates, the overlap with the bridge increases causing an increase in the interaction of the two sites. A one electron transition is equivalent to moving an electron from one site to the other.

2. Transition Dipole Moments and Spectra

The quantity that we examine in detail in this section is the transition dipole moment given by $\hat{\mu}_{i,j} = \int \Psi^i_{\text{el}} \boldsymbol{\mu}\cdot\mathbf{e} \Psi^j_{\text{el}}\, d\mathbf{r}$. In this paper we examine electronic transitions between states i and j, $\hat{\mu}_{i\neq j}$. The physical meaning of $\hat{\mu}_{i\neq j}$ for each of the three models of intervalence electron-transfer spectra can be explained in a simple way by using qualitative electron density diagrams to represent the ground and excited electronic states Ψ^i_{el} and Ψ^j_{el}. The electronic dipole moment operator $\boldsymbol{\mu}\cdot\mathbf{e}$ is represented by a function that changes sign at the origin. A similar pictoral representation was used by Tannor to illustrate the symmetries of the transition dipole moment in the water molecule.[30] Detailed considerations for the calculation of spectra using the time dependent theory have been previously discussed.[16,31−34] An overview of our implementation for mixed valence electronic spectra is presented in the Appendix.

Symmetry of $\hat{\boldsymbol{\mu}}_{i\neq j}$ and Spectra in the Coordinate-Displaced Model for *X*, *Y*, and *Z* Polarization. The pictorial representation of the transition dipole moment for the coordinate-displaced model is shown in Figure 3. The electron density of the ground electronic state of the molecule

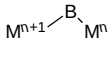

is shown at the top of the figure. The electron density is highest on the side of the molecule with the lowest positive charge and is represented by an ellipse. As the molecule vibrates, the ellipse elongates and contracts. The excited electronic state,

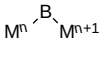

has its highest electron density on the right-hand side of the figure. It is represented by an ellipse, identical with that of the ground state, but located on the other side of the molecule. It also elongates and contracts as the molecule vibrates, but in the opposite sense.

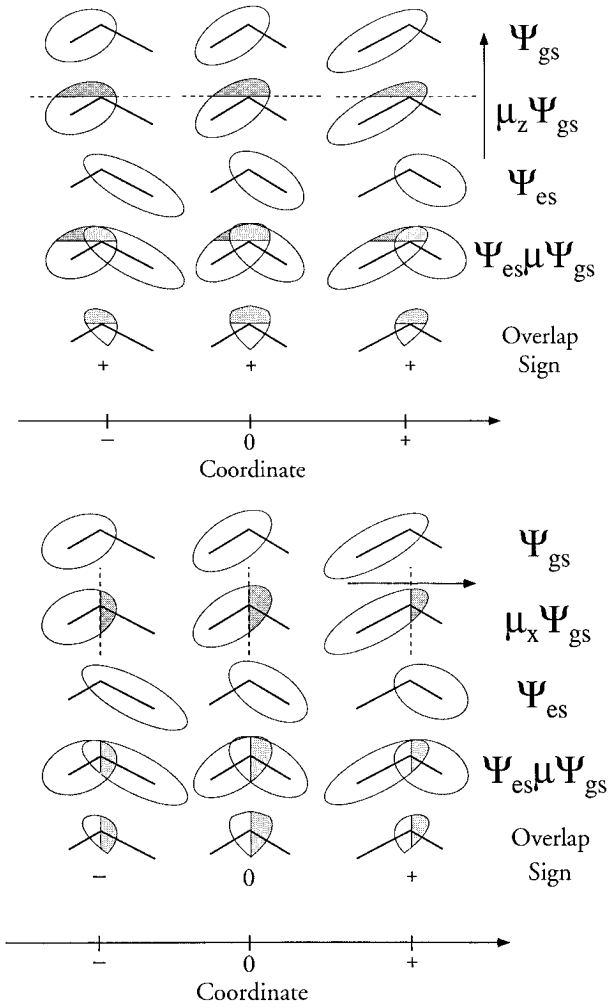

Figure 3. The top and bottom panels show the transition dipole moments as a function of coordinate for the coordinate displaced model for *X*- and *Z*-polarized light, respectively. The top line shows how the diabatic ground state localized on one site might vary with change in coordinate. The second line shows the interaction of this state with the vector potential of light as having placed a node in the electronic wave function. The third line shows the "excited state" as being the other trapped valence configuration. The fourth line shows the "doorway state" (line two) superimposed with the excited state (line 3). The fifth line shows just the overlap from line four. The sign of the transition dipole moment appears below line five.

To represent $\hat{\mu}_{i\neq j}$ for *Z*-polarized light (the direction that bisects the bond angle), the *Z* component of the electric dipole operator causes a sign change in the *Z* direction. Thus, $\mu_z \cdot \mathbf{e}\Psi^j_{el}$ is represented as the ellipse containing a nodal plane in the *XY* plane, a negative sign (shaded area) above the plane and a positive sign below the plane. The product $\Psi^i_{el}\mu\cdot\mathbf{e}\Psi^j_{el}$ is shown in the fourth row, and the overlap $\int\Psi^i_{el}\mu\cdot\mathbf{e}\Psi^j_{el}\,d\mathbf{r}$ in the bottom row.

Two important features of the overlap, the pictorial representation of the transition dipole moment, are that its sign does not change along the configurational coordinate, and that it is nonzero at $Q = 0$. The physical meaning is that the transition is electric dipole allowed at all positions along the coordinate.

In contrast, the pictorial representation for *X* polarization, shown in figure 3b, shows that the transition is dipole forbidden at $Q = 0$ but is allowed at other positions. The crucial feature, illustrated by the diagrams, is that the electric dipole operator for *X* polarization produces a nodal plane in the *YZ* plane in $\mu_x\cdot\mathbf{e}\Psi^j_{el}$, a negative sign to the right (shaded area) and a positive sign to the left. Thus the overlap, representing the transition dipole moment, is zero at $Q = 0$. As the molecule vibrates in the positive and negative directions, the contribution of the shaded area to the overlap respectively increases and decreases causing $\hat{\mu}_{i\neq j}$ to change sign. The interpretation of this behavior of $\hat{\mu}_{i\neq j}$ is that the transition is electric dipole forbidden at $Q = 0$ but vibronically allowed.

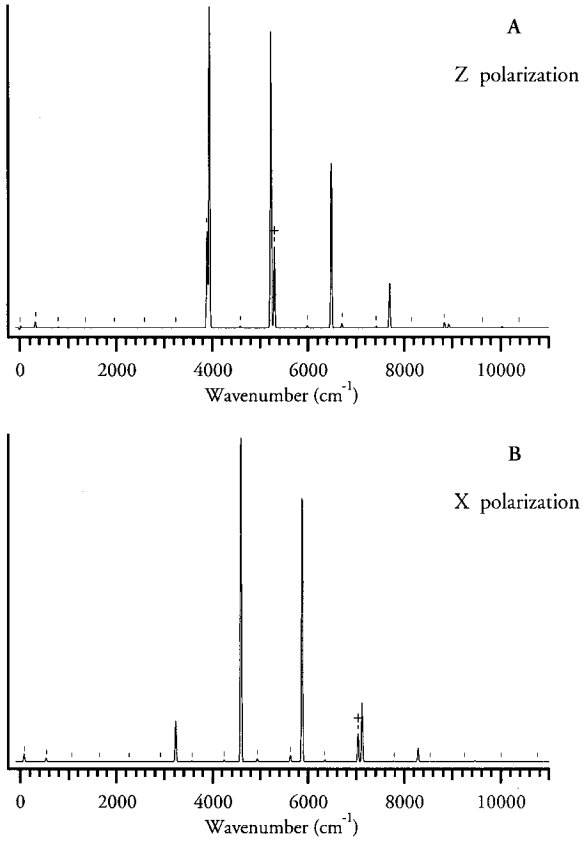

Figure 4. Absorption spectra generated from the coupled diabatics under the coordinate displaced model for *Z*-polarized light, top, and *X*-polarized light, bottom.

The spectrum (calculated as described in the appendix) for *Z*-polarized light in Figure 4a shows two regions. The low-energy region consists of bands with even changes in quantum number. The high-energy region peaks at the $\nu = 1$ quantum and is non-Poisson. The most intense peaks in the high energy region have an odd integer change in quantum number and the components of the total wave function from each surface have their relative phase changed by π as compared to the ground-state eigenfunction. The peaks marked with | are from the "ground-state". Note that the "ground-state" peaks are enhanced because of the coupling to the "excited state" peaks, particularly the $\nu = 3$ upper state peak marked with a dagger.

For light polarized in the *Y* direction, the node is placed in the *XZ* plane and the overlap is zero and remains zero along *Q*. The transition is forbidden in this polarization direction.

The spectrum for *X*-polarized light in Figure 4b also shows two regions. The low-energy region consists of bands with odd changes in quantum number. The high energy region peaks at the $\nu = 2$ quantum and is also non-Poisson. The most intense peaks in the high energy region have an even integer change in quantum number and the components from each surface of the total wave function have the same relative phase as the ground-state eigenfunction. The peaks marked with | from the "ground state" are again enhanced by the "excited state" peaks when they are close in energy (e.g., the $\nu = 6$ upper state peak marked with †).

Symmetry of $\hat{\mu}_{i\neq j}$ and Spectra in the Energy-Displaced Model for *X*, *Y*, and *Z* Polarization. For the energy-displaced model, the one-electron transition occurs from a bonding orbital

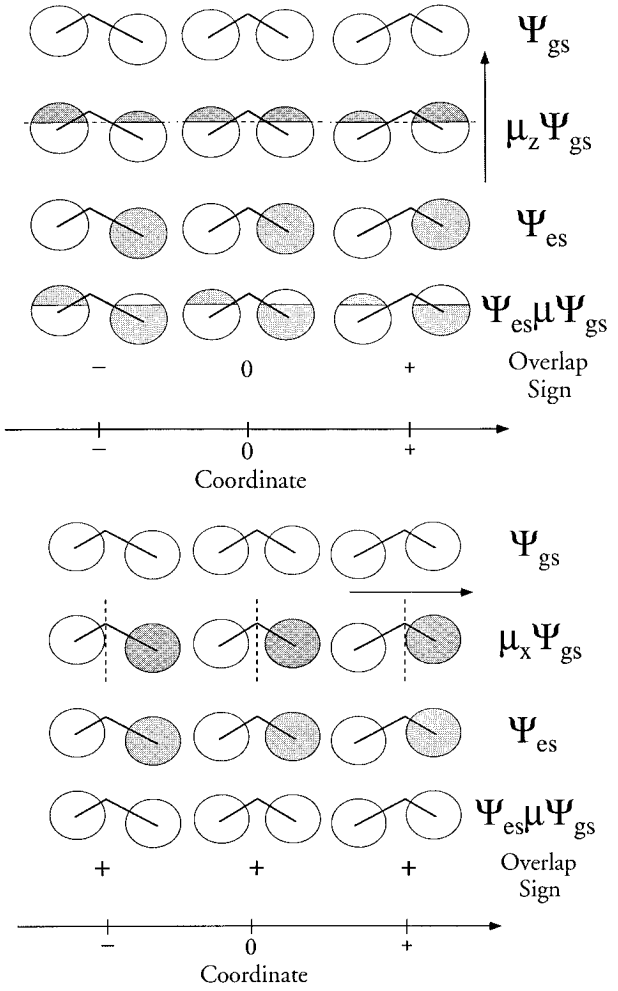

Figure 5. The top and bottom panels show the transition dipole moments as a function of coordinate for the energy displaced model for *X*- and *Z*-polarized light, respectively. The top line shows how the diabatic bonding ground state might vary with change in coordinate. The second line shows the interaction of this state with the vector potential of light as having placed a node in the electronic wave function. The third line shows the "excited state" as being the antibonding combination of basis states. The fourth line shows the "doorway state" (line two) superimposed with the excited state (line 3). Just below line four is the sign of the transition dipole moment.

(labeled +) to an antibonding orbital (labeled −). Figure 5 schematically shows the behavior of the transition dipole moment. The bonding orbital is represented by two equal in-phase circles on each side of the molecule. As the molecule vibrates, one circle moves toward the center of the molecule as the other moves away from the center. Light polarized in the *Z* direction places a node in the orbital as shown in the second line of the figure. The antibonding orbital, shown in the third line, is represented by two out-of-phase circles. The overlap $\hat{\mu}_{i\neq j}$ is shown in the bottom line. The overlap is zero at the origin but becomes nonzero as the molecule vibrates. Note that the overlap changes sign at the origin. This behavior is interpreted as an electric dipole forbidden, vibronically allowed transition.

The representation for *X*-polarized light is shown in Figure 5b. In this case the *X* component of the electric dipole operator places a node in the *XY* plane as shown in the second line. The overlap is thus positive everywhere. The magnitude of the overlap changes along the normal coordinate, but the sign is constant. This behavior corresponds to an electric dipole allowed transition.

For light polarized in the *Y* direction, the node is placed in the *XZ* plane and the overlap is zero and remains zero along *Q*. The transition is forbidden in this polarization direction.

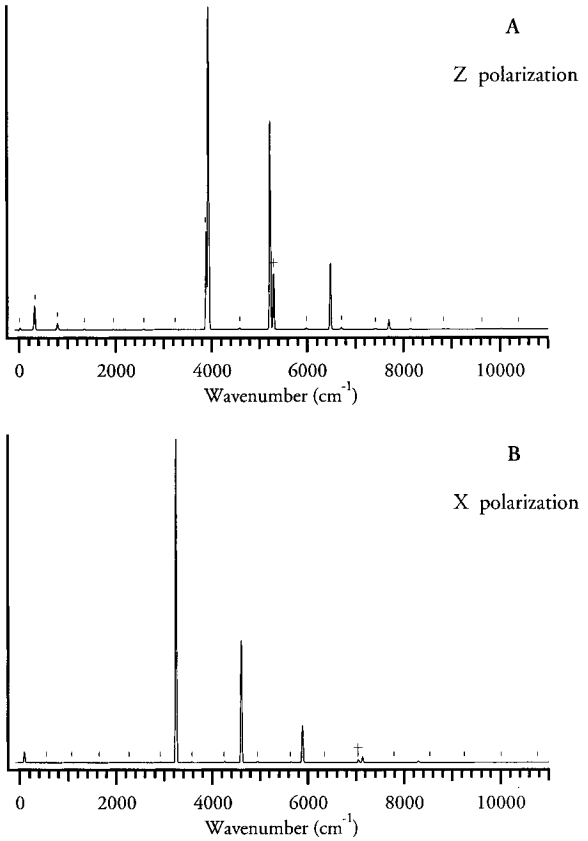

Figure 6. Absorption spectra generated from the coupled diabatics under the energy displaced model for *Z*-polarized light, top, and *X*-polarized light, bottom.

The spectrum for *Z*-polarized light in Figure 6a shows two regions. The low-energy region consists of bands whose eigenfunctions have even changes in quantum number and have the majority of their probability density on the lower diabatic. The upper surface eigenfunction component has one more node than the lower surface component. The high-energy region peaks at the $\nu = 1$ quantum and is somewhat non-Poisson. The most intense high-energy region peaks have eigenfunctions with an odd integer change in quantum number and have the majority of their probabilty density on the upper diabatic. The upper surface eigenfunction component has one fewer node than the lower surface component, which is opposite of the low-energy features. The peaks marked with | are from the "ground state". Note that the "ground state" peaks are enhanced by the "excited state" peaks, particularly the $\nu = 3$ upper state peak (marked by †).

The spectrum for *X*-polarized light in Figure 6b shows two regions. The low-energy region consists of bands with odd changes in quantum number and have the majority of their probabilty density on the lower diabatic. The upper surface eigenfunction component has one more node than the lower surface component. The high energy region peaks at the $\nu = 0$ quantum. The most intense high energy region peaks have an even integer change in quantum number and have the majority of their probabilty density on the upper diabatic. The upper surface eigenfunction component has one fewer node than the lower surface component which is opposite of the low energy features. The peaks marked with | from the "ground state" are again enhanced by the "excited-state" peaks when they are close in energy, e.g., the $\nu = 6$ upper state peak marked by a dagger.

Symmetry of $\hat{\mu}_{i\neq j}$ and Spectra in the Nondisplaced Model for *X*, *Y*, and *Z* Polarization. The pictorial representation of the transition dipole moment for the non-displaced model is very similar to that shown in Figure 3. This representation is

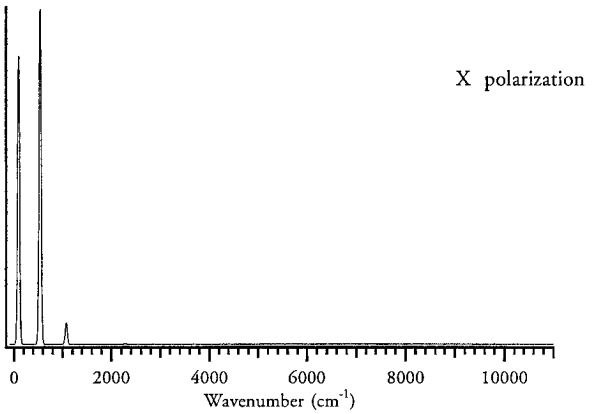

Figure 7. Absorption spectrum generated from the coupled diabatics under the nondisplaced model for *X*-polarized light. For comparison, the scale of the wavenumber axis is the same as those in Figures 4 and 6.

very similar to that of model 1 with one major difference: the minimum of the energy of the elipse representing the electron probability is at the origin of the configurational coordinate. Thus both the ground and the excited electronic states are undisplaced in both energy and coordinate. The interpretation of the overlap is the same as that discussed for the coordinate displaced model. For *Z*-polarized light, the overlap is positive everywhere along the coordinate, whereas for *X*-polarized light it changes sign at the origin.

The intervalence spectrum for the *X* polarization is shown in Figure 7. The spectrum consists of a single low energy region with $\Delta\nu = 1, 3, 5$, etc. They are vibronic transitions that occur in the infrared region of the spectrum, but they do not arise from pure vibrational transitions. The calculated spectrum for the *Z* polarization consists of a single line at zero energy, i.e., no transition.

Symmetry of $\hat{\mu}_{i\neq j}$ and Spectra in the Adiabatic Model for *X*, *Y*, and *Z* Polarization. The symmetries of $\hat{\mu}_{i\neq j}$ can be pictorally represented in the same manner as those in the energy displaced model (Figure 5.) Thus, if the Condon approximation is made for an allowed transition, the polarization direction is *X*. For a dipole forbidden vibronically allowed transition, $\hat{\mu}_{i\neq j}$ changes sign at the origin of the configurational coordinate and the polarization direction is *Z*.

The spectrum for *Z*-polarized light in Figure 8a shows one region. This region peaks at the $\nu = 3$ quantum and is non−Poisson. The peaks have an odd integer change in quantum number. The spectrum for *X*-polarized light in Figure 9b also shows a single region. The spectrum peaks at the $\nu = 0$ quantum and is also non-Poisson. The corresponding eigenfunctions have an even integer change in quantum number.

Note that we see no intensity borrowing or enhancement of the peaks from the "ground" state in the spectrum. In the adiabatic limit there cannot be a contribution to the spectrum from the highly vibrationally excited ground state because there is no coupling of the two states. Note also that the energies are different from those calculated for models 1 and 2 and that the intensities of the vibronic bands in the absorption spectrum are different for these models, even though both of these diabatic models give the same adiabatic potential energy surface as that used in this section.

3. Relationships and Connections between the Models

Unitary Transformations and Eigenvalues. Diagonalization of the diabatic potential energy matrix results in the adiabatic potential energy matrix. All three models diagonalize to the same adiabatic potential energy matrix. However since

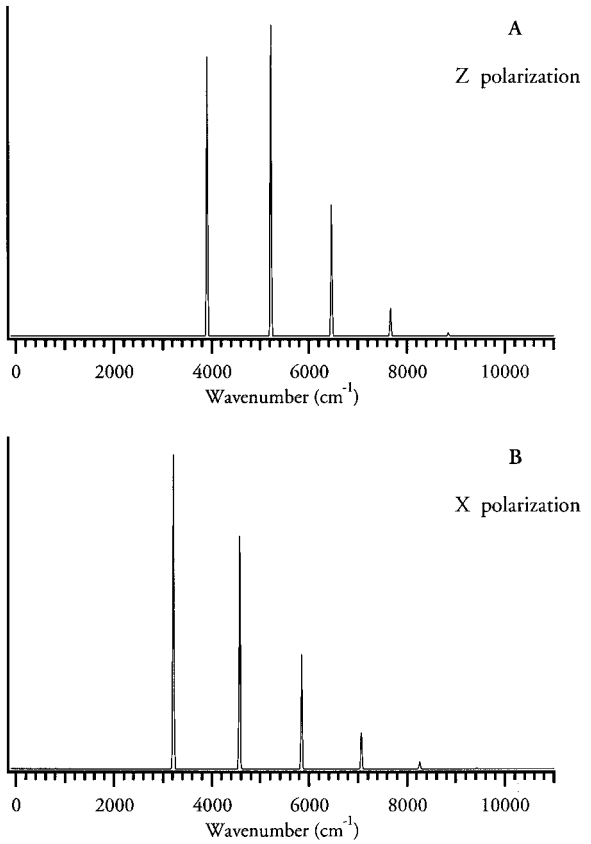

Figure 8. Absorption spectra generated from the uncoupled adiabatics for *Z*-polarized light, top, and *X*-polarized light, bottom.

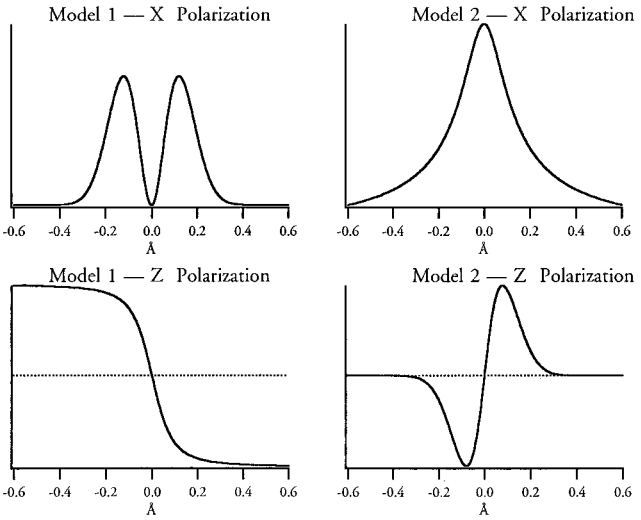

Figure 9. Plots of the off-diagonal elements of the transition dipole as a function of coordinate in the adiabatic basis which arise from unitary transformation of the diabatic basis dipoles as described in section 3. Model 1 *X* polarization is shown at top left. Model 1 *Z* polarization is shown at bottom left. Model 2 *X* polarization is shown at top right. Model 2 *Z* polarization is shown at bottom right.

the diabatic models are different, the eigenvectors and therefore the unitary transformation matrices differ. The diabatic-to-adiabatic unitary transformation is defined by the following relationship:

$$\hat{\mathbf{V}}_A = \mathbf{U}^\dagger \hat{\mathbf{V}}_D \mathbf{U} \tag{4}$$

where $\hat{\mathbf{V}}_A$ is the adiabatic potential energy operator, $\hat{\mathbf{V}}_D$ is the diabatic potential energy operator, and $\hat{\mathbf{U}}$ is the unitary transformation matrix:

$$\hat{\mathbf{U}} = \hat{\mathbf{U}}^{\dagger} = \begin{vmatrix} C_a & C_b \\ C_b & -C_a \end{vmatrix} \tag{5}$$

For model 1

$$ {}_1C_a = \left(kQ\Delta Q - \sqrt{(\Delta QkQ)^2 + \epsilon^2}\right)\Big/ {}_1N$$

$$ {}_1C_b = \epsilon/{}_1N \tag{6}$$

$$ {}_1N = \sqrt{\left(kQ\Delta Q - \sqrt{(\Delta QkQ)^2 + \epsilon^2}\right)^2 + \epsilon^2}$$

For model 2

$$ {}_2C_a = \left(\epsilon - \sqrt{(\Delta QkQ)^2 + \epsilon^2}\right)\Big/ {}_2N$$

$$ {}_2C_b = kQ\Delta Q/{}_2N \tag{7}$$

$$ {}_2N = \sqrt{\left(\epsilon - \sqrt{(\Delta QkQ)^2 + \epsilon^2}\right)^2 + (kQ\Delta Q)^2}$$

For model 3

$$ {}_3C_a = {}_3C_b = 1/\sqrt{2} \tag{8}$$

For the purpose of our calculations, these matrices transform the diabatic Hamiltonian to the adiabatic Hamiltonian:

$$\hat{\mathbf{H}}_{\mathrm{A}} = \mathbf{U}^{\dagger}\hat{\mathbf{H}}_{\mathrm{D}}\mathbf{U} \tag{9}$$

where $\hat{\mathbf{H}}_{\mathrm{A}}$ is the Hamiltonian with a diagonal adiabatic potential energy operator and $\hat{\mathbf{H}}_{\mathrm{D}}$ has coupled diabatic potentials. Although these transformations diagonalize the potential energy matrix, they leave coupling terms in the kinetic energy operator, some of which depend on first derivatives with respect to coordinate or momentum. Some of these coupling terms do not depend on coordinate derivatives of the nuclear wave function and therefore are more appropriately included in the potential energy operator. After the transformation

$$\hat{\mathbf{T}}_{\mathrm{A}} = \mathbf{U}^{\dagger}\hat{\mathbf{T}}_{\mathrm{D}}\mathbf{U} \tag{10}$$

the kinetic energy operator becomes

$$\hat{\mathrm{T}}_{\mathrm{A}} = -\frac{1}{2m}\left(\nabla^2 + 2\begin{vmatrix} C_a\nabla C_a + C_b\nabla C_b & C_a\nabla C_b - C_b\nabla C_a \\ C_a\nabla C_b - C_b\nabla C_a & C_a\nabla C_a + C_b\nabla C_b \end{vmatrix}\nabla + \begin{vmatrix} C_a\nabla^2 C_a + C_b\nabla^2 C_b & C_a\nabla^2 C_b - C_b\nabla^2 C_a \\ C_a\nabla^2 C_b - C_a\nabla^2 C_a & C_a\nabla^2 C_a + C_b\nabla^2 C_b \end{vmatrix}\right) \tag{11}$$

Since the unitary transformation matrix for model 3 to the adiabatics is coordinate independent, $\mathbf{T}_3$ commutes with $\hat{\mathbf{U}}$ and $\hat{\mathbf{U}}^{\dagger}$ and therefore

$$\hat{\mathbf{T}}_{\mathrm{A}} = \mathbf{U}^{\dagger}\mathbf{U}\hat{\mathbf{T}}_3 = \hat{\mathbf{T}}_3 \tag{12}$$

The above analysis emphasizes the relationships between the eigenvalues when nonadiabatic effects are represented by coupled diabatic potentials. Since the kinetic energy operator is assumed to be diagonal in the diabatic basis, the residual coupling terms that are not transformed away can lead to differences between the eigenvalues of different representations. The implicit neglect of these terms in diabatic calculations results in the Hamiltonians being different. The presence of these residual coupling terms depends only on the type of unitary transformation that connects the two models in question. If the unitary transformation matrix is coordinate independent, $\hat{\mathbf{T}}$ commutes with $\hat{\mathbf{U}}$ and $\hat{\mathbf{U}}^{\dagger}$, there are no residual momentum coupling terms to neglect and therefore both representations give the same eigenvalues.

The eigenvalues from model 3 and the adiabatic limit are identical. The models are related under eqs 4 and 5 using the eigenvectors defined by eq 8. Since this is a coordinate-independent unitary transformation, the eigenvalues calculated under these two models are the same. Models 1 and 2 are both related to the adiabatic limit by coordinate dependent unitary transformations. Therefore the eigenvalues of models 1 and 2 will differ from those in the adiabatic limit. The relationship between models 1 and 2 is defined by eqs 4, 5, and 8. Since this is a coordinate-independent transformation, calculations using the assumption of a diagonal kinetic energy operator will generate identical eigenvalues. By analogy to model 3 and the adiabatics, this analysis illustrates why models 1 and 2 give the same energies.

Transition Dipole Moments. The transition probabilities are dependent upon the eigenfunctions of the model in question and the transition dipole moments. Much literature has been devoted to calculating mixed-valence transitions under model 2 using the Condon approximation for the diabatic electronic transition.[35−44] The symmetry of this choice of dipole moment is consistent with what we have defined as the *X*-polarization direction and is appropriate for calculating the spectra of linear molecules. The Condon approximation is used because it physically represents an "allowed" transition and because little is known about the coordinate dependence of the transition dipole moment. In matrix form the diabatic electronic transition dipole for model 2 and *X* polarization is

$$\hat{\mu}_2^X = \begin{vmatrix} 0 & \mu_{(Q)}^{\mathrm{even}} \\ \mu_{(Q)}^{\mathrm{even}} & 0 \end{vmatrix} \tag{13a}$$

When the Condon approximation for the diabatic electronic transition is made in model 1 it is consistent with what we have defined as *X* polarization. To calculate a charge-transfer spectrum under model 1 for the *X* polarization, the Condon approximation cannot be used because the transition dipole moment must change sign at the origin as derived in section 2. In matrix form the diabatic electronic transition dipole moment for model 1 and *X* polarization is

$$\hat{\mu}_1^X = \begin{vmatrix} 0 & f_{(Q)}^{\mathrm{odd}} \\ f_{(Q)}^{\mathrm{odd}} & 0 \end{vmatrix} \tag{13b}$$

When the transition dipole moment for *X* polarization is transformed from the model 2 basis to the model 1 basis

$$\hat{\mu}_{2\rightarrow 1}^X = \mathbf{U}^{\dagger}\hat{\mu}_2^X\mathbf{U} = \begin{vmatrix} \mu_{(Q)}^{\mathrm{even}} & 0 \\ 0 & -\mu_{(Q)}^{\mathrm{even}} \end{vmatrix} \neq \hat{\mu}_1^X = \begin{vmatrix} 0 & f_{(Q)}^{\mathrm{odd}} \\ f_{(Q)}^{\mathrm{odd}} & 0 \end{vmatrix} \tag{14}$$

model 2's transformed transition dipole matrixes are not the same as those from model 1. In fact, since the transformed transition dipole moment matrix has only diagonal elements it does not even represent an electronic transition in this basis. This conclusion should be expected because the physical meaning of the transition in model 1 is different from that of model 2. It is important to point out that limiting the calculation to model 2 tacitly makes an assumption as to the nature of the electronic transition and therefore has limited scope and applicability.[29,46,47]

It is interesting to note that $\hat{\mu}_{i=j}$, a diagonal μ matrix, in a coupled system, gives rise to a spectrum when used with the time-dependent theoretical methods in Appendix 1. For completeness we show the full dipole matrix including terms from both electronic diabatic transitions (off-diagonals) and vibrational diabatic transitions (diagonals). For model 1:

$$\hat{\mu}_1^X = \begin{pmatrix} g_{(Q)} & f_{(Q)}^{\text{odd}} \\ f_{(Q)}^{\text{odd}} & -g_{(-Q)} \end{pmatrix} \qquad \hat{\mu}_1^Z = \begin{pmatrix} g_{(Q)} & f_{(Q)}^{\text{even}} \\ f_{(Q)}^{\text{even}} & g_{(-Q)} \end{pmatrix}$$

For model 2:

$$\hat{\mu}_2^X = \begin{pmatrix} f_{(Q)}^{\text{even}} & \mu_{(Q)}^{\text{odd}} \\ \mu_{(Q)}^{\text{odd}} & -f_{(Q)}^{\text{even}} \end{pmatrix} \qquad \hat{\mu}_2^Z = \begin{pmatrix} f_{(Q)}^{\text{odd}} & \mu_{(Q)}^{\text{even}} \\ \mu_{(Q)}^{\text{even}} & -f_{(Q)}^{\text{odd}} \end{pmatrix}$$

with

$$\mu_{(Q)}^{\text{even}} = g_{(Q)} - g_{(-Q)} \qquad \mu_{(Q)}^{\text{odd}} = g_{(Q)} + g_{(-Q)}$$

Of course, the spectra generated using the diagonal elements, $\mu_{i=j}$, in a given model are the same as the spectra generated using the off-diagonal elements, $\mu_{i\neq j}$, for the model related to it by a coordinate-independent unitary transformation. For example; the spectrum arising from these diagonal elements for *X* polarization in model 1 is the same as the spectrum for *X* polarization for model 2. The symmetry of the diagonal elements of the dipole matrix, representing diabatic vibrational transitions, can be derived in a similar manner to that of the off-diagonal elements.

Group Theoretical Connections between the Models. The diabatic electronic transition dipole moments for *X*- and *Z*-polarization directions are model dependent. For *X* polarization in models 1 and 3, $\mu_{i\neq j}$ changes sign at the origin of the configurational coordinate, whereas for model 2 and the adiabatic potential model it does not change sign. Relationships between the transition dipole moments are derived by using the unitary transformation matrixes that relate the models as shown in the previous section. However, the transformation often does not provide a physically meaningful $\mu_{i\neq j}$ for electronic transitions in the new diabatic basis, even though a spectrum can be calculated by using it. A specific example is the transformation of the transition dipole moment for *X* polarization for model 2 to model 1; the Condon approximation in model 2 transforms to a form that does not represent electron transfer in model 1. In all of the models, however, the presence or absence of a given vibronic band in the spectra must obey the constraints imposed by group theory. In this section we show that the calculated spectra do obey those constraints and explain the results in terms of both the familiar C_{2v} point group symmetry and the more general nuclear permutation inversion group symmetry model.[47]

The symmetry properties can be analyzed from two different points of view: interchange symmetry or point-group symmetry. The complete nuclear permutation inversion symmetry group for two identical sites has the following symmetry elements: *E*-identity; (12)-permutation; *E**-inversion; (12)*-permutation−inversion. The appropriate character table is given in Table 1. The top row gives the appropriate symmetry operations in the (12)* molecular symmetry group. The second line gives the equivalent point symmetry operations for the C_{2v} point group.

The Condon approximation, that the transition dipole moment is constant over the coordinates being considered in the calculation, is the most commonly used approximation for dipole allowed electronic transitions and is implicitly used in most Franck−Condon calculations of vibronic intensity. For polarization directions where our analysis shows that the transition dipole moment does not change sign, we use this approximation because the exact functional form of $\mu_{i\neq j}$ is not known beyond the basic symmetry requirements (i.e., presence or lack of a sign change). It is important to note that the Condon approximation corresponds to *Z* polarization in models 1 and 3 and *X* polarization in model 2 and the adiabatic model. The group theoretical explanation is straightforward.

TABLE 1

Γ	E	(12)	E^*	(12)*	
C_{2v}	E	C_2	$\sigma_v(xz)$	$\sigma_v(yz)$	
A_1	1	1	1	1	T_z
A_2	1	1	−1	−1	
B_1	1	−1	1	−1	T_x
B_2	1	−1	−1	1	T_y

Model 1 is based on two sites that must preserve interchange symmetry. Two states, labeled 1 and 2, correspond to trapped valence states with the extra electron on site 1 and 2 respectively. For these two states to couple via the coordinate independent coupling term they must transform (in this molecular symmetry group) as the same irreducible representation. Therefore, the transition dipole integral is

$$\left\langle \Gamma_{\Psi_1} \middle| \begin{matrix} A_1 \\ B_1 \\ B_2 \end{matrix} \middle| \Gamma_{\Psi_2} \right\rangle$$

with $\Gamma_{\Psi_1} = \Gamma_{\Psi_2}$. Clearly the only transition that is allowed when the Condon approximation is used is along the electric dipole moment that makes the integral transform as A_1. The electric dipole operator for *Z* polarization transforms as A_1.

Model 2 is also subject to the restraints of group theory. The two states labeled + and − correspond to states where the "extra" electron is in a bonding or antibonding orbital, respectively. For these two states to couple via the linear in *Q* coupling term, + and − must transform (in this molecular symmetry group) as A_1 and B_1 respectively. Therefore, the dipole integral is

$$\left\langle \Gamma_{\Psi_+} \middle| \begin{matrix} A_1 \\ B_1 \\ B_2 \end{matrix} \middle| \Gamma_{\Psi_-} \right\rangle$$

with $\Gamma_{\Psi_+} = A_1$ and $\Gamma_{\Psi_-} = B_1$. This integral transforms as A_1 when the electric dipole operator is B_1. Thus the Condon approximation polarization direction is *X*.

The symmetry considerations for model 3 are very similar to those appropriate for model 1. The two diabatic surfaces represent trapped valences that have their energy minima at the same position on the configuration coordinate. They must transform as the same irreducible representation. The analysis of the transitions is the same as that for model 1 and yields *Z* polarization for the Condon approximation.

In the adiabatic model, the electronic states transform as A_1 and B_1. When the Condon approximation is used, the allowed polarization direction is *X*.

The presence or absence of a specific vibronic band in the absorption spectra for a particular polarization direction of the light is consistent for the three diabatic models and the adiabatic model. The important unifying feature is the total symmetry of the initial and final states. The total symmetry depends on both the symmetry of the electronic state and on the symmetry of the vibrational wave function. In all of the models, the vibrational coordinate under consideration is B_1 and the

vibrational eigenfunctions will have either B_1 or A_1 symmetry. For light polarized in the *Z* direction, nonzero intensities are found only for transitions between states of the same total symmetry whereas for *X* polarization, nonzero intensities are found only for transitions between states of different total symmetries. A specific example in the calculated spectra is the band at 4590 cm^{-1} in models 1 and 2 that is present in *X* polarization in both models and absent in *Z* polarization. In model 1 it is interpreted as "allowed" in the Condon approximation, whereas in model 2 it has zero intensity in the Condon approximation. Thus, even though the transition dipole moments for a given polarization direction may have different symmetries in the different models, the presence or absence of a given vibronic band in a given polarization direction is the same.

When the dipoles used in the calculation of spectra in Figures 4 and 6 are transformed to the adiabatic limit, it is clear that their symmetry properties are consistent with the observation that the spectral lines observed depend only upon symmetry and the polarization of light and do not depend on the model chosen. Figure 9 (top) shows the transition dipole moments for *X* polarization that result upon unitary transformation to the adiabatic representation for the coordinate-displaced model and the energy-displaced model respectively. Figure 9 (bottom) show the *Z*-polarization results. Only the off-diagonal elements are shown since they are what generate an electronic transition. Once in the adiabatic representation, the transition dipole moment for a given polarization has the same symmetry with respect to the coordinate. Both *Z*-polarization transition dipole moments are odd, whereas both *X*-polarization transition dipole moments are even. Thus, even though the functional form for the transition dipole moment for a given polarization is different in the different models, and even though the polarization direction consistent with the Condon approximation is different, the group theoretical requirements are retained.

Conclusions

Four model potential energy surfaces representing different physical meanings of intervalence electron transfer spectra are presented. The spectra resulting from the models are calculated by using the time dependent theory of electronic spectroscopy. The simplest model is based on electronic transitions between adiabatic potential energy surfaces. The three different models based on diabatic surfaces displaced in coordinate, displaced in energy, and nondisplaced give the identical surfaces used in the adiabatic model when specific forms of coupling are chosen. The adiabatic potential does not uniquely define a diabatic representation. The functional forms of the electronic transition dipole moments appropriate for each model in the three orthogonal polarization directions are derived by using a physically intuitive graphical method. The functional forms must be judiciously chosen because the usual assumptions for uncoupled surfaces (e.g., the Condon approximation for an electric dipole allowed transition) may imply different polarization directions in the different models. We explicitly show how the functional forms, the symmetries, and the definitions of allowed and forbidden are dependent on the polarization direction and how they differ for each of the models. Each of the models gives a different calculated spectrum although the diabatic surfaces displaced in coordinate and displaced in energy have the same eigenvalues, and the adiabatic model and the diabatic model with nondisplaced surfaces have the same eigenvalues. Even though the functional forms of the transition dipole moment are different in the different models, and even though the interpretation of "allowed" and "forbidden" transitions can interchange, the group theoretical requirements for the presence or absence of a given band in a given polarization direction of the incident light are the same. Calculated fits to experimental spectra must be recognized as being dependent on both the choice of the model and the transition dipole moment and must be interpreted cautiously.

Appendix: Calculation of Spectra Using the Time-Dependent Theory

In this Appendix the theoretical foundation underlying the calculation of intervalence band spectra in the framework of the time dependent theory of molecular spectroscopy is briefly presented. The most important quantity in the calculation is the time evolution of the wavepacket on the excited state diabatic potential surfaces $|\vec{\Phi}(t)\rangle$. $|\vec{\Phi}(t)\rangle$ is a vector quantity with a component for each of the electronic states in the calculation and is a function of the configurational coordinate *Q*. The initial wavepacket for our calculations is given by

$$|\vec{\Phi}(t=0)\rangle = \hat{\mu}_{i,j}|\vec{\chi}\rangle \tag{A1}$$

where $\mu_{i=j}$ is the electronic transition dipole moment. The transition dipole moments $\mu_{i=j}$ are discussed in section 2 of this paper. For transition dipole moments that do not change sign along the coordinate *Q*, the Condon approximation ($\mu_{i=j}$ = constant) is used. For those that do change sign, the functional form

$$\hat{\mu}_{i\neq j} = (e^{\kappa(Q+\Delta)^2} - e^{\kappa(Q-\Delta)^2})\cdot\begin{vmatrix}0 & 1\\ 1 & 0\end{vmatrix} \tag{A2}$$

is used because it has the desired symmetry property and also approaches zero at long bond lengths. The parameters used for calculations in this paper were $\Delta = 0.15$ Å and $\kappa = \bar{\nu}m/4R_\infty m_e N_A a_0^2$ where $\bar{\nu}$ =100 cm^{-1}; m = 17 g/mol; R_∞ is the Rydberg constant in cm^{-1}; N_A is Avagadro's number; m_e is the mass of an electron in grams; a_0 is the Bohr radius in Å. To carry out a quantitative calculation for a specific molecule, neither of these approximations is exact, and explicit forms of $\hat{\mu}_{i,j}$ must be determined from electronic structure calculations.

The eigenfunction χ_{ω_j} corresponding to the eigenvalue ω_j is filtered from the propagating wavefunction using eq A3.21 $\Phi(t)$

$$\chi_{\omega_j} = |\Phi(\omega_j)\rangle = \int_0^\infty e^{-i\omega_j t}|\Phi(t)\rangle\, dt \tag{A3}$$

is the time-dependent (propagating) wave function and ω_j is the eigenvalue. For coupled diabatic potentials, each eigenfunction χ_{ω_j} is an array with two components corresponding to the two diabatic potentials which form the basis in all of our calculations. Eigenfunctions of all of the thermally populated eigenstates, weighted by their thermal populations, are needed in order to calculate the temperature dependence of the spectra.

The absorption spectrum in the time dependent theory is calculated by using equation A4,16−18 with $I(\omega)$ the absorption at frequency ω and $\langle\Phi|\Phi(t)\rangle$ the autocorrelation function of the initial wavepacket $\langle\Phi(0)|$ and the wavepacket $|\Phi(t)\rangle$ that evolves with time. For two coupled diabatic potential surfaces, the situation that is used to treat intervalence absorption bands, two wavepackets, $|\Phi_A(t)\rangle$ and $|\Phi_B(t)\rangle$ moving on the two coupled diabatic potential surfaces, are needed.[31−33] The total overlap $\langle\Phi|\Phi(t)\rangle$ is

$$I(\omega) \propto \omega \int_{-\infty}^{\infty} e^{i\omega t}\langle\Phi|\Phi(t)\rangle\, dt \tag{A4}$$

$$\langle\Phi|\Phi(t)\rangle = \langle\Phi_A|\Phi_A(t)\rangle + \langle\Phi_B|\Phi_B(t)\rangle \tag{A5}$$

To calculate the autocorrelation function in eq A3, we need $|\Phi(t)\rangle$, the propagating wave function in the two coupled diabatic potential surfaces. It is given by the time-dependent Schrödinger equation for two coupled states:

$$i\frac{\partial\vec{\Phi}}{\partial t} = \hat{\mathbf{H}}\vec{\Phi}$$

with

$$\vec{\Phi} = \begin{vmatrix}\Phi_A\\ \Phi_B\end{vmatrix} \qquad \hat{\mathbf{H}} = \begin{pmatrix}H_A & V_{AB}\\ V_{BA} & H_B\end{pmatrix} \tag{A6}$$

where $H_i = -(1/2m)\nabla^2 + V_i(Q)$ denotes the Hamiltonian, $V_i(Q)$ is the potential energy as a function of the configurational coordinate Q, $-(1/2m)\nabla^2$ the nuclear kinetic energy, and $V_{AB} = V_{BA}$ is the coupling between the two diabatic potentials (chosen to be coordinate independent for the coordinate displaced model, linear for the energy displaced model, etc.) For simplicity, harmonic diabatic potentials were used in all of the examples, although the theoretical method is not restricted by the functional form of the diabatic potentials. The diabatic potentials are given by eqs 1−3.

The split operator method developed by Feit and Fleck is used to calculate $|\Phi(t)\rangle$.[21−23] Both the configurational coordinate Q and the time are represented by a grid with points separated by ΔQ and Δt, respectively. For one diabatic potential surface, the time-dependent wave function $|\Phi(t + \Delta t)\rangle$ is obtained from $|\Phi(t)\rangle$ by using the equation

$$|\Phi(t+\Delta t)\rangle = \mathrm{e}^{-i\hat{\mathbf{V}}\Delta t/2}\,\mathrm{e}^{-i\hat{\mathbf{T}}\Delta t}\,\mathrm{e}^{-i\hat{\mathbf{V}}\Delta t/2}|\Phi(t)\rangle + O(\Delta t^3) \tag{A7}$$

For the case of two coupled diabatic potentials, the exponential operators $\hat{\mathbf{T}}$ and $\hat{\mathbf{V}}$ in eq A7 are replaced by 2×2 matrices operating simultaneously on $|\Phi_A(t)\rangle$ and $|\Phi_B(t)\rangle$:

$$\hat{\mathbf{V}} = \begin{pmatrix}V_A & V_{AB}\\ V_{BA} & V_B\end{pmatrix} \qquad \hat{\mathbf{T}} = -\frac{\nabla^2}{2m}\begin{pmatrix}1 & 0\\ 0 & 1\end{pmatrix} \tag{A8}$$

Details of the computer implementation of eq A7 are given in the literature.[21−23,31−33,48−52]

It is interesting to note the different roles of $\hat{\mathbf{T}}$ and $\hat{\mathbf{V}}$. $\hat{\mathbf{T}}$, the momentum operator, transfers wave function amplitude $\Phi_i(t)$ among grid points along Q at each time step but does not transfer amplitude between the diabatic surfaces. These changes are easily monitored by looking at the wavepacket $\Phi_i(t)$ after every time step. On the other hand, $\hat{\mathbf{V}}$, the potential energy operator, changes the momentum and transfers amplitude between the diabatic surfaces at each time step, but does not couple grid points along Q. The amplitude transfer between the diabatic potentials can be followed by calculating the norms $\langle\Phi_A(t)|\Phi_A(t)\rangle$ and $\langle\Phi_B(t)|\Phi_B(t)\rangle$ after every time step. The norms are a quantitative measurement for the amount of population change between the two states. In the case of the symmetric intervalence transition for models 1 and 3, no net population change occurs.

Both operators $\hat{\mathbf{T}}$ and $\hat{\mathbf{V}}$ affect the total overlap $\langle\vec{\Phi}|\vec{\Phi}(t)\rangle$ in eq A5 and therefore the absorption spectrum. For this reason the adiabatic approximation is incorrect. Only the calculation which simultaneously involves both coupled diabatic surfaces according to eq A8 gives the correct total overlap.

Acknowledgment. This work was made possible by a grant from the National Science Foundation (CHE94-07289).

References and Notes

(1) *Mixed Valence Compounds*; Brown, D. B., Ed.; Reidel: Dordrecht, 1980.
(2) Robin, M. B.; Day, P. *Adv. Inorg. Radiochem.* **1967**, *10*, 247.
(3) Hush, N. S. *Prog. Inorg. Chem*. **1967**, *8*, 391.
(4) Hush, N. S. *Chem Phys*. **1975**, *10*, 361.
(5) Allen, G. C.; Hush, N. S. *Prog. Inorg. Chem*. **1967**, *8*, 357.
(6) Clark, R. J. H. *Chem. Soc. Rev.* **1984**, *13*, 219.
(7) Blondin, G.; Girerd, J. J. *Chem. Rev*. **1990**, *90*, 1359.
(8) *Mixed Valency System: Applications in Chemistry, Physics and Biology*; Prassides, K., Ed.; NATO ASI Series C; Kluwer: Dordrecht, 1991; Vol. 343.
(9) Crutchley, R. J. *Adv. Inorg. Chem*. **1994**, *41*, 273.
(10) Blasse, G. *Struc. Bonding* **1991**, *76*, 153.
(11) Taylor, P.; Beattie, J. K.; Hush, N. S. *Inorg. Chem*. **1976**, *15*, 992
(12) Bersuker, I. B.; Borshch, S. A. *Adv. Chem. Phys.* **1992**, *81*, 703.
(13) Vincent, J. B.; Christou, B. *Adv. Inorg. Chem.* **1989**, *33*, 197.
(14) Wieghardt, K. *Angew. Chem., Int. Ed. Engl.* **1989**, *28*, 1153.
(15) Que, L., Jr.; True, A. E. *Prog. Inorg. Chem.* **1990**, *38*, 98.
(16) Simoni, E.; Reber, C.; Talaga, D.; Zink, J. I. *J. Phys. Chem*. **1993**, *97*, 12678.
(17) Kosloff, R.; Ratner, M. A. *J. Chem. Phys.* **1982**, *77*, 2841.
(18) Heller, E. J. *J. Chem. Phys.* **1975**, *62*, 1544.
(19) Heller, E. J. *J. Chem. Phys.* **1978**, *68*, 3891.
(20) Heller, E. J. *Acc. Chem. Res.* **1981**, *14*, 368.
(21) Feit, M. D.; Fleck, J. A.; Steiger, A. *J. Comput. Phys.* **1982**, *47*, 412.
(22) Kosloff, D.; Kosloff, R. *J. Comput. Phys.* **1983**, *52*,35.
(23) For an introductory overview see Tanner, J. J. *J. Chem. Educ.* **1990**, *67*, 917.
(24) Alvarellos, J.; Metiu, H. *J. Chem. Phys*. **1988**, *88*, 4957.
(25) Thompson, T. C.; Truhlar, D. G.; Mead, C. A. *J. Chem. Phys*. **1985**, *82*, 2392.
(26) Pacher, T.; Cederbaum, L. S.; Köppel, H. *Adv. Chem. Phys.* **1993**, *84*, 293.
(27) Köppel, H; Domke, W.; Cederbaum, L. S. *Adv. Chem. Phys.* **1984**, *57*, 59.
(28) Fulton, R. L.; Gouterman, M. *J. Chem. Phys.* **1961**, *35*, 1059.
(29) Schatz, P. N.; Piepho, S. B. *J. Phys. Chem*. **1994**, *98*, 11226.
(30) Tannor, D. J. *J. Phys. Chem*. **1988**, *92*, 3341.
(31) Reber, C.; Zink, J. I. *J. Chem. Phys*. **1992**, *96*, 2681.
(32) Reber, C.; Zink, J. I. *J. Phys. Chem*. **1992**, *96*, 571.
(33) Wexler, D.; Zink, J. I.; Reber, C. *J. Phys. Chem*. **1992**, *96*, 8757.
(34) Reber, C.; Zink, J. I. *Comments Inorg. Chem*. **1992**, *13*, 177.
(35) Piepho, S. B.; Krausz, E. R.; Schatz, P. N. *J. Am. Chem. Soc*. **1978**, *100*, 2996.
(36) Wong, K. Y.; Schatz, P. N.; Piepho, S. B. *J. Am. Chem. Soc*. **1979**, *101*, 2793.
(37) Prassides, K.; Schatz, P. N. *J. Phys. Chem.* **1989**, *93*, 83.
(38) Tsukerblat, B. S.; Palii, A. V.; Gamurar, V. Y.; Berengolts, A. S.; Kishinevsky, H. M. *Phys. Lett. A* **1991**, *158*, 341.
(39) Piepho, S. B. *J. Am. Chem. Soc.* **1990**, *112*, 4197.
(40) Larsson, S. *J. Am. Chem. Soc.* **1981**, *103*, 4034.
(41) Ko, J.; Ondrechen, M. J. *Chem. Phys. Lett*. **1984**, *112*, 507.
(42) Ondrechen, M. J.; Ko, J.; Root, L. J. *J. Phys. Chem.* **1984**, *88*, 5919.
(43) Zhang, L. T.; Ko, J.; Ondrechen, M. J. *J. Phys. Chem. 93*, **1989**, 3030.
(44) Ondrechen, M. J.; Ferretti, A.;Lami, A.;Villani, G. *J. Phys. Chem.* **1994**, *98*, 11230.
(45) Ferretti, A.; Lami, A.; Ondrechen, M. J.; Villani, G. *J. Phys. Chem.* **1995**, *99*, 10485.
(46) Talaga, D.; Reber, C.; Zink, J. I. *J. Phys. Chem*. **1994**, *98*, 11233.
(47) Bunker, P. R. *Molecular Symmetry and Spectroscopy*; Academic: Orlando, FL, 1979.
(48) Heather, R.; Metiu, H. *J. Chem. Phys*. **1989**, *90*, 6903.
(49) Jiang, X. P.; Heather, R.; Metiu, H. *J. Chem. Phys*. **1989**, *90*, 2555.
(50) Zhang, J.; Heller, E. J.; Huber, D.; Imre, D. G.; Tannor, D. *J. Chem. Phys*. **1988**, *89*, 3602.
(51) Das, S.; Tannor, D. J. *J. Chem. Phys*. **1989**, *91*, 2324.
(52) Zhang, J.; Heller, E. J.; Huber, D.; Imre, D. G. *J. Phys. Chem*. **1991**, *95*, 6129.

JP951165A